Characterization of the Deflections of a Catheter Steered Using a Magnetic Resonance Imaging System

Frédérick P. Gosselin, Viviane Lalande, and Sylvain Martel*
École Polytechnique de Montréal
Nanorobotics Laboratory
Pavillon Lassonde, local M-4505
2500, chemin de Polytechnique
Montréal, Qc, Canada, H3T 1J4
(Dated: December 13, 2010)

Purpose: We quantify the deflections of a catheter and a guidewire in MR setting with different designs of ferromagnetic tips and a system of high gradient coils which can generate gradients, and thus forces, 20 times larger than a conventional scanner.

Methods: Different designs of catheter tips are experimentally tested in an effort to maximise the deflections. One to two ferromagnetic spheres are attached at the distal tip of the catheter (or guidewire) with different spacing between the spheres. The effect of dipole-dipole interaction on the steering of the catheter is studied through experimentation and theoretical modelling. The effect of using many spheres on the artefact generated in fast imaging sequences is also investigated.

Results: A catheter and a guidewire are successfully steered by applying magnetic gradients inside a magnetic resonance scanner. More ferromagnetic material allows for larger magnetic forces, however the use of two ferromagnetic spheres introduces undesired dipole-dipole interactions. Two ferromagnetic spheres generate a single larger artefact as they are close together.

Conclusion: By varying the distance between the two ferromagnetic spheres, a balance can be struck between the need to minimise the size of the tip and the undesirable dipole-dipole interaction.

I. INTRODUCTION

Success of catheterization procedures is strongly dependent on the manoeuvrability of the catheter employed and requires physicians to possess a high level of endovascular skills which can only be obtained through specialised training. The complexity of intravascular procedures increases with the tortuosity of the vessel network, the distance of the location to be reached from the percutaneous access point as well as the nature of the treatment [1, 2]. Navigation is traditionally done using different preformed or shapeable guidewires and catheters which can slide inside one another. The physician transmits movements from the proximal end of the catheter outside the patient to the distal one through the control of two degrees of freedom: a linear back and forth movement and a rotation of the catheter about its axis. The placement of the catheter in a 3D network using this limited actuation can lead to many complications: longer procedure time, more radiation, hematoma and vessel puncture [1, 3].

Many actuation systems have been devised to address this lack of control over the steering of the catheter [2]. Mechanical actuation performed with pull-wires placed inside the lumen is available [4]. However, due to the complexity of the catheter design, miniaturization is difficult and because of the cost of manufacturing, the catheter is non-disposable. Magnetic actuation has the inherent benefit of taking the control system out of the catheter itself and can thus offer greater miniaturization possibilities. Such a magnetic catheter platform exists [5–7] and consists in large external magnets placed besides the operating table that are moved using computer control to generate a torque on smaller magnets at the tip of the catheter. This allows the operator to angle and steer the catheter inside the patient.

For both of these actuations principles as well as in traditional catheterization, the progress of the catheter inside the patient is monitored using X-ray fluoroscopy. This has the drawback of causing radiation exposure to both the patient and the physician. This introduces the need for the latter to wear a heavy lead apron.

Lately, several interventional endovascular procedures have been done using magnetic resonance imaging (MRI) to visualize the catheter placement [3, 8–10]. MRI has the advantages over x-ray angiography of not emitting ionizing radiation and having both three-dimensional visualization and soft tissue imaging capabilities. Whereas fluoroscopy only allows to delineate the lumen of the vessels, MRI has the potential to visualize the morphology of soft tissues surrounding the blood vessel.

To improve on the possibilities of MR-guided intravascular procedures, ideas have been presented to steer a catheter inside a scanner using wound coils [11, 12]. By passing an electrical current in the coils at the tip of the catheter, a magnetic field is created which interacts with the permanent field of the MR scanner. This interaction generates a steering torque on the catheter which tends to align the magnetic moment of the catheter with the permanent magnetic field of the MRI apparatus. With three orthogonal coils on its tip, the catheter can be steered in space by applying current to the proper coils. However,

* Corresponding author: sylvain.martel@polymtl.ca ; http://www.nano.polymtl.ca

since the steering principle works by aligning the magnetic field of the catheter with that of the MR scanner, it is thus impossible to generate torques parallel to the direction of the permanent magnetic field. Moreover, the radio frequencies used for imaging and the intermittent current passing through the coils induce ohmic heating of the catheter wiring. Recent research efforts show that this problem could be alleviated by dissipating the heat using saline coolant flowing within the lumen of the steerable catheter [13, 14].

A new actuation system has been proposed that actively makes use of the hardware of the MRI apparatus for steering. To acquire an image, the MR scanner executes a sequence of fast changing magnetic field gradients. These gradients can generate significant forces on a ferromagnetic body upon being arranged in a proper steering sequence [15]. By alternating a steering sequence with a tracking sequence, a MR scanner was used to steer and track a bead inside the carotid artery of a living swine [16, 17]. It was later shown that this principle of propulsion with MRI gradients could be used to deflect a catheter [18–20]. This actuation system is fundamentally different from the previously discussed magnetic systems [5, 6, 11, 12] as it employs magnetic gradient forces rather than magnetic field–aligning torques.

The feasibility of bending a catheter with the gradients of MR scanners has been shown [18–20]. However, no quantitative data on the bending of catheters or guidewires with this principle exist in the literature. Zhang et al. [20] proposed a well integrated imaging and steering system for the control of a catheter, however they also showed that the maximum force a conventional MR scanner could exert on a ferromagnetic bead is equal to 0.36 times the weight of the bead. In many cases is not enough to overcome the natural bend a catheter might have.

To combine steering and tracking of a catheter with the same apparatus, certain aspects of the tracking must be considered. First off, the presence of a large ferromagnetic body in the bore of the scanner can significantly distort the image through the creation of an artefact. This artefact makes imaging difficult in the vicinity of the ferromagnetic body but it also allows fast positioning of the bead by locating the artefact itself rather than imaging the catheter. In fact, to allow interleaving the propulsion and tracking sequences, tracking must be done very fast. The Magnetic Signature Selective Excitation (MS-SET) sequence was designed for that purpose [17, 21]. MS-SET is based on either a spin echo or gradient echo sequence in which the frequency of the RF excitation has been offset to that of a magnetic equipotential curve corresponding to the artefact. It is fast as it only requires scanning three lines of the k-space to obtain 3-D positioning of the artefact due to the ferromagnetic body.

Secondly, although the gradients of the tracking sequence can potentially influence the position of the catheter, in practice the tracking sequence can be designed to minimise these effects by nulling all gradient moments [17]. As for movement happening *during* the application of the gradients, significant displacement is unlikely because the duration of the strongest gradients is of the order of a few milliseconds. For example, considering the acceleration a clinical scanner can exert on a ferromagnetic bead is 0.36 times the gravitational acceleration [20], and considering that the strongest gradients in a MS-SET sequence last less than a millisecond [17], we can expect that a free ferromagnetic bead would move by an amount $\frac{1}{2}\times 0.36\times 9.81\times 0.001^2 \approx 2\times 10^{-6}$ m. Even if the gradient lasted ten times longer, the displacement of the free ferromagnetic bead would be less than a millimetre. By properly designing the tracking sequence, it is possible to allow interleaving of steering and tracking sequences as it has been done in the past [16, 17, 20].

It is the purpose of this paper to propose a quantification of catheter and guidewire deflections attainable in MR setting with different designs of ferromagnetic tips and a system of high gradient coils which can generate gradients (and thus forces) 20 times larger than a conventional apparatus. To push further our understanding of magnetic catheter steering, we develop a theoretical model based on non-linear beam theory coupled with a magnetic dipole formulation. Moreover, we look at the effect of using multiple beads of ferromagnetic material on the deflections attainable with the catheter and the artefact this creates on MR images.

The materials and method used as well as the reasoning behind the magnetic tip designs are presented in Section II followed by the derivation of the theoretical model in Section III. The results of the deflection experiments and simulations along with MR images of the artefact created by the catheter tips are presented in Section IV. A discussion of the main results concludes the paper in Section V.

II. EXPERIMENTAL METHOD

The experiment aims at designing a magnetic tip maximising the deflections of a clinical catheter (or guidewire). For that, we must quantify these deflections using magnetic fields inside a MR scanner. The working principle used to bend the catheter is shown on the schematic of Fig. 1. The catheter is equipped with a ferromagnetic tip at it free end and is clamped at a distance ℓ from its distal end. The ferromagnetic material at the tip of the catheter is magnetised by the scanner's permanent field $\vec{B}_0$ (measured in Teslas, T) aligned with the z-axis. Upon application of a magnetic gradient $\vec{\nabla}\vec{B}$, a magnetic force is generated on the ferromagnetic body:

$$\vec{F}_m = V\left(\vec{M}\cdot\vec{\nabla}\right)\vec{B}, \tag{1}$$

where V and $\vec{M}$ are respectively the volume and the volumetric magnetisation of the ferromagnetic material.

To maximise the magnetic force, three parameters must be maximised: the volume of ferromagnetic mate-

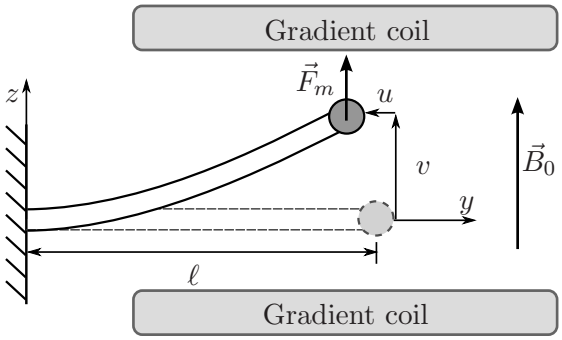


FIG. 1. Schematic diagram of the catheter deformed by the application of a magnetic force due to a magnetic gradient produced by a pair of Maxwell coils. The whole assembly is placed inside the bore of a MR scanner. The z-direction is defined along the permanent magnetic field of the scanner.

rial, the magnetisation of the material and the intensity of the magnetic gradient.

The volume of ferromagnetic material at the tip of the catheter is limited by size constraints. The catheter tip must be smaller than the targeted blood vessel. Moreover, the ferromagnetic material must be shaped to minimise anisotropy. When placed in a strong magnetic field, the ferromagnetic material is magnetised in such a way as to minimise its energy. Magnetisation occurs in the easiest direction and if that direction is not aligned with the magnetic field, a torque tends to align it:

$$\vec{T}_m = V\vec{M} \times \vec{B}. \tag{2}$$

In our force actuated system, this torque creates a parasitic bend in the catheter and must be minimised. To do so, we shape the ferromagnetic material into a sphere. However, even when shaped as a sphere, ferromagnetic material still has a preferential magnetisation direction due to the crystalline anisotropy of the material. To completely get rid of parasitic torques, we enclose the ferromagnetic sphere inside a rigid casing that allows it to rotate freely. The volume of ferromagnetic material is thus limited to a sphere of diameter smaller than the blood vessel. In the present study, all experiments are performed with spheres of ferromagnetic material of diameter $d = 1.5$mm and weight of 0.0146g. To increase further the volume of ferromagnetic material, we investigate the possibility of using multiple spheres at the tip of the catheter. The use of many magnetic dipoles introduces possible interactions causing parasitic torques, however these can be controlled by varying the distance between the dipoles.

In the strong magnetic field of MR scanners, ferromagnetic materials reach their saturation magnetisation. Therefore, a 3 T scanner offers no advantage in terms of magnetic steering over a 1.5 T scanner. In both fields, the ferromagnetic material is saturated. Thus, the ideal material to actuate the catheter has a high saturation magnetisation. Materials with the highest saturation magnetisation are iron-cobalt alloys. For example, Permendur has a saturation magnetisation of 1.91×10^6 A/m [22]. However, iron-cobalt alloys are brittle and difficult to machine into small spheres while keeping their magnetic properties. We thus used beads made of chrome steel provided by Salemball (Salem Specialty Ball Co., Canton, CT). From vibrating sample magnetometer measurements (Walker Scientific, Worchester, MA), we know that the beads have a magnetisation of 1.30×10^6 A/m.

Since the beads are magnetised to saturation along the direction of the permanent magnetic field of the scanner, their magnetisation can be written as

$$\vec{M} = M_s\vec{e}_z. \tag{3}$$

From Maxwell's equations, the curl of the magnetic field is nil. We can thus define $G_x = \partial B_z/\partial x = \partial B_x/\partial z$, $G_y = \partial B_z/\partial y = \partial B_y/\partial z$ and $G_z = \partial B_z/\partial z$ [23]. We express the three components of magnetic forces of Eq. 1 using Eq. 3 as

$$\vec{F}_m = VM_s \left\{ \begin{array}{ccc} G_x & G_y & G_z \end{array} \right\}^{\mathrm{T}}. \tag{4}$$

In the clinical 1.5 T Siemens Sonata MR scanner used in the present experiments, the maximal intensity of magnetic gradient attainable is 40 mT/m. At such a high value of gradient intensity, the duty cycle must be kept very small for continuous application. In our tests and similarly to Zhang et al. [20], the effective magnetic gradient—equal to the product of the magnetic gradient times the duty cycle—cannot be much higher than 20 mT/m. To reach values of gradient of 400 mT/m, we use a pair of custom Maxwell coils which can be inserted inside the bore of the scanner. The coils are designed such that they can carry their maximal rated current at full duty cycle for several minutes.

The use of gradient amplitudes much larger than those found in traditional MRI applications raises safety concerns. High amplitude magnetic gradients with fast switching rates can lead to peripheral nerve stimulation (PNS) [24, 25]. To avoid PNS, the rate of change of the magnetic gradient $\partial G_z/\partial t$ should be kept below 20 T/s [24]. For a set of coils generating three orthogonal gradients of 400 mT/m each, creating a norm of 693 mT/m, the rise time should be at least 35 ms. For catheter steering, this limit on how fast the magnetic force can be applied is acceptable and can easily be dealt with as we can expect the navigation through a bifurcation to last several seconds.

Always in the aim of maximising deformation amplitudes, the FasTracker microcatheter (Boston Scientific, Natick, MA) and the Glidewire MRI compatible guidewire (Terumo, Somerset, NJ) were chosen for their small diameter and low bending rigidity. The Fastracker catheter has an outer diameter 0.83 mm at its distal end (2.5 Fr) and a bending rigidity $EI = 1.2 \times 10^{-6}$ Nm^2. The Glidewire guidewire has an outer diameter 0.46 mm at its distal end (1.4 Fr) and a bending rigidity $EI = 0.4 \times 10^{-6}$ Nm^2. The bending rigidities of the

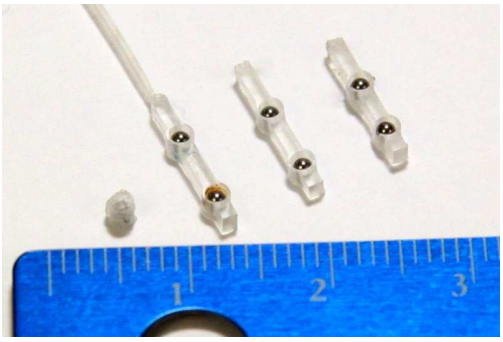


FIG. 2. Photograph of the ferromagnetic tips C1/G1, C2, C3, C4 shown from left to right. The ruler in the picture is graduated in centimetres. Note that for testing, the open holes of the sphere casings were sealed shut with tape.

catheter and the guidewire were evaluated by considering them as a cantilever Euler-Bernoulli beam [26] and measuring the deflection caused by various weights attached to the free end. Note that the bending rigidity had a significant variation depending on the orientation. The rigidity was lowest when bending in the plane the catheter (and the guidewire) is wound for storage. In the perpendicular plane, bending rigidity was higher. We used the lower values as our experiments were conducted in the lower rigidity plane.

The tested tip designs are shown on Fig. 2. Catheter tips with one or two magnetic spheres were tested. For the tips with multiple spheres, the spacing between the spheres was varied from $r = 4.5$ mm to $r = 6$ mm measured centre to centre. The tips are 1.9 mm thick and 2.1 mm wide at the location of a sphere. The varied parameters of the different configurations tested are listed in Table I.

The deflection tests were performed in a water bath to reduce friction. The setup is placed between the Maxwell coils along the axis of the permanent field of the MR scanner (z-axis). The gradient field is cycled from 0 to 400 mT/m in the positive and negative z-direction in steps of 22 mT/m. The gradient is applied continuously and the static deformations are measured from photographs taken with a MRI compatible camera (MRC systems GmbH, Heidelberg, Germany).

Ferromagnetic beads distort the magnetic field inside the scanner and create large artefacts in MR images which greatly limit the possibility of imaging the anatomy in their vicinity. However the artefact can be used for tracking [16, 20, 21]. Currently, the custom high-gradient coils do not allow us to perform imaging sequences when they are in place inside the scanner. Our eventual goal is to interleave the tracking and propulsion sequences but for the moment we must perform both tasks separately due to hardware limitations. To insure that the tracking sequences previously used to track and steer a bead with a conventional scanner can function with the use of multiple beads we obtained images from our catheter tips with a clinical Siemens Sonata scanner without the custom coils. We imaged tips C1 and C2 inside a phantom made of a rubber tube shaped into a ring of 80 mm diameter. The TurboFLASH and MS-SET sequences were performed on each tip to compare their artefact. The TurboFLASH images were obtained in the coronal plane with a flip angle of 5 °, a field of view of 200 mm by 200 mm, resolution 192 by 192, TE = 1.44 ms, TR = 2000 ms and a slice thickness of 20 mm. With the MS-SET sequence [21], although only three projections are required to position the artefact in space, full images were obtained in the coronal plane using a field of view of 200 mm by 200 mm, resolution 256 by 256, an offset frequency of 1 kHz, TE = 22 ms and TR = 89 ms.

Before showing the results of the experiments, the theoretical model is derived in the following section.

III. THEORETICAL MODELLING

To confirm that the catheter and the guidewire behave as cantilever beams subjected to an end force and to better understand the magnetic interaction happening when multiple spheres are used to deflect the catheter, we develop a simple theoretical model of the deflection of the catheter.

We consider a catheter tip composed of two identical soft ferromagnetic spheres free to rotate independently inside a rigid casing. The model can later be simplified to the case of a single sphere. To evaluate the magnetic forces on the catheter tip inside the bore of the scanner, we model the two spheres as magnetic dipoles of strength m which we label A and B as shown in Fig. 3. Since the spheres are free to rotate in the casing, we assume that their magnetisation is aligned with the permanent field of the scanner, i.e., $\vec{m} = m\vec{e}_z$. At the distances we are interested in, the permanent field of the scanner is much stronger than the magnetic field of one of the dipoles. We can therefore neglect the effect dipole A has on the magnetisation of dipole B and vice versa. Nevertheless, as shown in Fig. 3 (a), dipole B which is located at $\vec{r}$ relative to dipole A perceives the magnetic field of dipole A [27]

$$\vec{B}_{\mathrm{BA}} = \frac{\mu_0 m}{4\pi r^3}\left[-\vec{e}_z + 3\left(\vec{e}_z \cdot \vec{e}_r\right)\vec{e}_r\right], \tag{5}$$

where $\mu_0 = 4\pi \times 10^{-7}$ Tm/A is the permeability of free space.

The force exerted on dipole B due to the magnetic field of dipole A is obtained by substituting Eq. 5 into Eq. 1:

$$\vec{F}_{\mathrm{BA}} = \frac{3\mu_0 m^2}{4\pi r^4}\left[\left(1 - 3\sin^2\theta_e\right)\vec{e}_r + \sin 2\theta_e \vec{e}_\theta\right], \tag{6}$$

where $\pi/2 - \theta_e$ is the angle between the magnetisation direction $\vec{e}_z$ and the position vector $\vec{r}$. By antisymmetry, $\vec{F}_{\mathrm{BA}} = -\vec{F}_{\mathrm{AB}}$.

Since the two spheres are enclosed in a rigid casing, they cannot move with respect to each other and

TABLE I. Details of the four tested experimental configurations on the catheter and the one configuration on the guidewire along with maximum deflection results.

Configurations	Number of spheres, n	Free length, L (mm)	Sphere spacing, r (mm)	Magnetic gradient, G_z (mT/m)	Tip deflection, v (mm)
C1	1	32.5	–	352	9.9
C2	2	32.0	6.0	352	17.0
C3	2	32.7	5.25	352	18.2
C4	2	32.7	4.5	352	20.3
G1	1	20.1	–	440	6.1

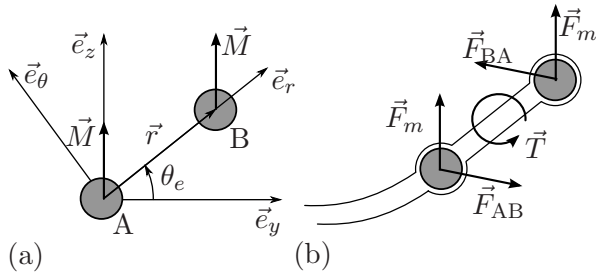


FIG. 3. Schematic diagram of the dipole model of the ferromagnetic spheres. In (a) the relative position of dipoles A and B is shown, while in (b) the forces and the resulting torque are depicted.

their attractive-repulsive components of force cancel out. However, their components of force perpendicular to $\vec{r}$ create a torque on the catheter tip

$$\vec{T} = \vec{r} \times \vec{F}_{\rm BA} = \frac{3\mu_0 m^2}{4\pi r^3} \sin 2\theta_e \vec{e}_x, \tag{7}$$

where $\vec{e}_x = \vec{e}_y \times \vec{e}_z$ is the direction sticking out of the paper in Fig. 3.

In our model, the dipoles represent spheres of ferromagnetic material magnetised to saturation in the z-direction, $\vec{m} = M_s V \vec{e}_z$, where $V = \pi d^3/6$. Eq. 1 of the force due to a magnetic gradient can be reformulated as

$$\vec{F}_m = \frac{\pi d^3}{6} M_s G_z \vec{e}_z, \tag{8}$$

where G_z is the magnetic gradient produced by the Maxwell coils. The force of Eq. 8 and the torque of Eq. 7 act on the catheter which can be modelled as a Euler-Bernoulli beam of uniform flexural rigidity EI. Assuming the beam inextensible for the range of forces studied here, the shear force along the beam is equal to the normal component of the force applied at the tip [26]

$$EI \frac{\partial^2 \theta}{\partial s^2} = -n F_m \cos\theta, \tag{9}$$

where n is the number of magnetic dipoles (1 or 2), $\theta = \theta(s)$ is the angle describing the deformation of the beam, and s is the lagrangian coordinate defined along the length of the beam from its clamped end to its free end. The boundary conditions are different depending on if there is only one dipole or two. If there is only one dipole, the boundary conditions are simply

$$\theta|_{s=0} = 0, \;\; EI \frac{\partial \theta}{\partial s}\bigg|_{s=\ell} = 0, \tag{10}$$

where ℓ is the length between the clamped end and the centre of the dipole at the free end. For two dipoles, the boundary conditions include the torques on the tip of the catheter

$$\theta|_{s=0} = 0, \;\; EI \frac{\partial \theta}{\partial s}\bigg|_{s=\ell-r} = T \sin 2\theta_e + F_m r \cos\theta_e, \tag{11}$$

where θ_e is the angle of the beam at the free end. To simplify the analysis, we define the following dimensionless numbers:

$$\eta = \frac{\pi d^3 \ell^2 M_s G_z}{6EI}, \quad \kappa = \frac{\mu_0 \pi d^6 M_s^2}{48 EI \ell^2}, \quad \rho = \frac{r}{\ell}, \quad \zeta = \frac{s}{\ell}, \quad \xi = \frac{v}{\ell}. \tag{12}$$

The number of dipoles and the dimensionless force a dipole generates always appear together as a product $n\eta$ so n could have been included in the definition of the parameter η. However since the goal of our modelling is in part to assess the advantage of using more than one ferromagnetic sphere on the catheter, keeping n and η separate allows to discern more easily the effect of the number of spheres on the deflections in the results section.

Using the dimensionless numbers of Eqs 12, we can rewrite the governing equation 9 as

$$\frac{\partial^2 \theta}{\partial \zeta^2} = -n\eta \cos\theta, \tag{13}$$

using one of the following sets of boundary conditions depending on if there is one or two dipoles at the tip of the beam:

$$\theta|_{\zeta=0} = 0, \quad \frac{\partial \theta}{\partial \zeta}\bigg|_{\zeta=1} = 0, \tag{14a}$$

$$\theta|_{\zeta=0} = 0, \;\; \frac{\partial \theta}{\partial \zeta}\bigg|_{\zeta=1-\rho} = \frac{\kappa}{\rho^3} \sin 2\theta_e + \frac{n\eta\rho}{2} \cos\theta_e. \tag{14b}$$

Equations 13 and 14 can be solved numerically. We use the shooting method and guess the angle of the beam at the free end θ_e. We then treat the problem as an initial value problem and integrate the beam shape from its free end to its clamped end using the Runge-Kutta algorithm. The Müller algorithm is used to iteratively converge to the correct value of end angle θ_e. Once the deformation of the beam is found, it can be integrated to lead to the tip displacement in the transverse direction for the case with a single dipole and for the case with two dipoles, respectively:

$$\xi = \int_0^1 \sin\theta \, \mathrm{d}\zeta, \tag{15a}$$

$$\xi = \int_0^{1-\rho} \sin\theta \, \mathrm{d}\zeta + \rho \sin\theta_e. \tag{15b}$$

The experimentally measured deflections of the catheter and guidewire are compared with the theoretical predictions in the following section.

IV. RESULTS

Composite photographs of the deformed catheter are shown in Fig. 4 for a magnetic gradient incrementing from -352 mT/m at the bottom of the figure to 352 mT/m at the top in steps of 22 mT/m while displaying only one picture out of two for clarity. In Fig. 4 (a), the catheter is equipped with tip C2 while in (b), it is equipped with tip C4 which has a smaller spacing of the ferromagnetic spheres. For a large spacing of the magnetic spheres on the catheter tip (Fig. 4 a) or with a single sphere at the tip (not shown), the displacement changes progressively with the incrementing applied magnetic gradient. However, for a smaller spacing (Fig. 4 b), the catheter "jumps" accross the plane traced by its undeformed position and a range of small transverse amplitude cannot be observed.

The measured values of maximum tip displacement for the catheter and the guidewire for the five tested configurations are listed in Table I along with the corresponding applied magnetic gradient. For similar free lengths, configurations with two ferromagnetic spheres attained deflections approximately twice as large. However, the guidewire test is difficult to compare because a different free length was used. The comparisons are easier in Fig. 5 where the deflection results are presented in dimensionless form using the numbers of Eqs 12.

With the proper scaling, the measures of the displacement versus the applied magnetic force on the catheter (•) and the guidewire (■) are shown to collapse on a single curve in Fig. 5 (a). The slight discrepancy in slope is possibly due to errors on the measure of flexural rigidity. For the tests with a single bead in Fig. 5 (a), the deflection measurements shown no sign of hysteresis due to the freedom of the ferromagnetic sphere to rotate inside the casing and always be aligned with the permanent magnetic field of the scanner.

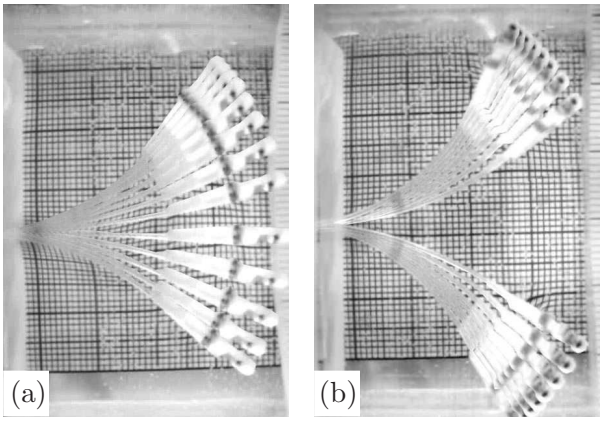


FIG. 4. Composite photographs of the deformation of the catheter subjected to a gradient incremented from -352 to 352 mT/m with tip C2 (a) and tip C4 (b).

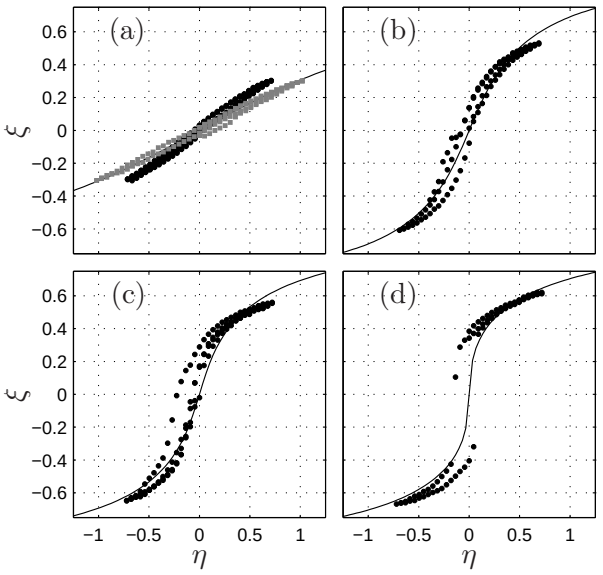


FIG. 5. Dimensionless plots of the tip displacement of the catheter (•) and guidewire (■) for varying transverse force for configurations C1 and G1 (a); C2 (b); C3 (c); C4 (d). The theoretical model is plotted in solid line: for one dipole (a); two dipoles with $\kappa = 0.00129$ and $\rho = 0.188$ (b); $\rho = 0.161$ (c); $\rho = 0.1138$ (d).

The use of a second ferromagnetic sphere at the tip of the catheter (Fig. 5 b-d) leads to dimensionless forces $n\eta$ twice as large for similar magnetic gradients. Accordingly, the measured deformations ζ for configurations C2, C3 and C4 are larger than for C1 by a factor of two approximately.

Moreover, the behaviour of the catheter with two ferromagnetic spheres is qualitatively different from that

equipped with a single sphere. For a single sphere (Fig. 5 a), in the range of values of η tested, the tip displacement is linearly proportional to the magnetic force. However the points corresponding to the tips with two spheres (Fig. 5 b-d) form an S that is more pronounced as the spacing is reduced. So much so that at a small enough value of the spacing ρ the catheter "jumps" accross the plane traced by its undeformed position as seen in the photographs of Fig. 4 (b).

The deformations computed with parameters corresponding to the experiments are plotted in Fig. 5 with solid lines. The model is in good quantitative agreement with the experiments for the single and multiple sphere configurations. It predicts well the change in behaviour due to the dipole interaction, i.e., the slope of ζ getting steeper at $\eta \sim 0$ for decreasing values of the spacing ρ.

The effect of the spacing of the dipoles on the steering of the beam is investigated further with the theoretical model. Using the same value of $\kappa = 0.00129$ as in the experiments, the deformation curves obtained with three representative spacing of the dipoles are plotted in Fig. 6. For large values of the spacing and therefore small dipole interaction(curve A), the deformation curve is smooth and progressive. For closer dipoles (curve B), the slope of the curve is steeper. However there is still only one equilibrium position possible per value of η. For dipoles very close together(curve C), their interaction becomes very strong. For a range of forces η between -0.57 and 0.57, many equilibrium position of ξ exist. In this range, two stable equilibrium positions (in solid line) and one unstable position (in dotted line) exist for each value of force. This is a non-linear behaviour that gives rise to jumps and hysteresis [28]. For example, consider the beam modelled in curve C. At $\eta = -1$, the tip deflection is $\xi = -0.66$. If the force is increased to $\eta = 0.5$ then the tip settles as $\xi = -0.35$. However, if the force is increased beyond $\eta = 0.57$, the model predicts that the beam jumps from $\xi = -0.25$ to 0.61.

This jump is quantified in Fig. 7 for varying values of the tip displacement. At large spacing values, no jump occurs. For $\rho < 0.131$, an increasing force causes the beam tip to jump from the position in dotted line to the displacement position indicated in solid line. For example, the jump amplitude of scenario C in Fig. 6 can be found at $\rho = 0.1$ in Fig. 7. For a decreasing force, the jump occurs in the opposite direction and the curves are symmetric about $\xi = 0$.

On Figures 5, we see that a gain in amplitude of deformation can be obtained through the use of two dipoles instead of one. However, in all tested configurations, the catheter (or guidewire) is initially perpendicular to the permanent field of the scanner. In that configuration, the magnetic torque generated by the dipole-dipole interaction tends to bend the beam away from its undeformed position. In the case where the catheter is initially parallel to the magnetic field, the dipole-dipole interaction would create a restoring torque. Our current experimental setup does not allow to test such configuration because the Maxwell coils only generate gradients in the direction of the permanent field.

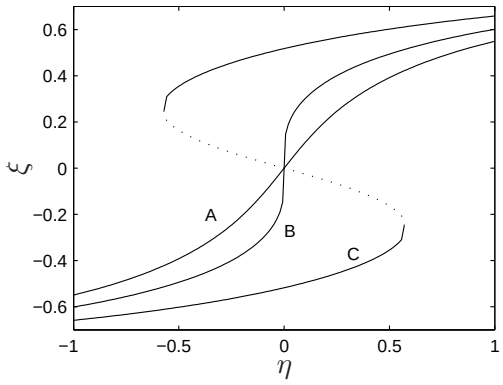


FIG. 6. Numerical solution of the tip displacement of the beam against transverse force for multiple dipoles with $\kappa = 0.00129$. Calculations are performed for a dipole spacing of $\rho = 0.16$ (A); $\rho = 0.13$ (B); $\rho = 0.10$ (C). The solid lines show the tip deflection corresponding to stable deformation while the dotted line of curve C corresponds to the unstable position.

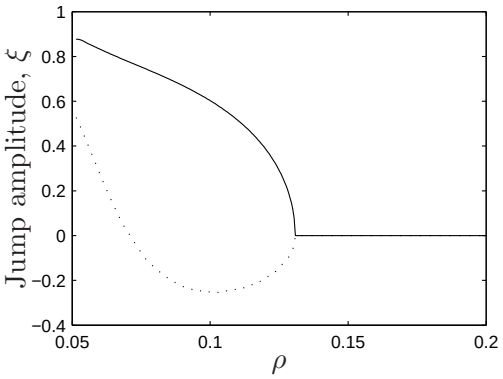


FIG. 7. Quantification of the non-linear jump in tip displacement for varying values of the spacing ρ between the two dipoles. The computations are done for a value of $\kappa = 0.00129$. For a catheter initially bent towards the negative z-direction, a force $n\eta$ in the positive z-direction induces a jump from the position indicated by the dash line to that indicated by the solid line. For $\rho > 0.131$, there is no jump.

However, we can easily test this configuration with the theoretical model by changing the sign of κ in Eq. 14. The results of these computations are shown in Fig. 8. The deformation curve obtained for a single dipole (solid line) is independent of the original orientation of the beam. For a beam with dipoles spaced by $\rho = 0.2$ (dash line), the amplitude is significantly larger than for a single dipole, but the gain is not as significant as when the beam is originally oriented perpendicular to the permanent field (Fig. 5). On the other hand, if the spacing between the dipoles is as small as $\rho = 0.1$ (dot line on Fig. 8), the restoring torque generated by the dipole-dipole interaction reduces the amplitude below that obtainable

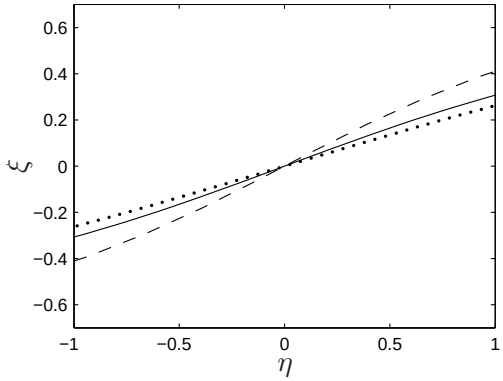


FIG. 8. Numerical solution of the tip displacement of the beam against transverse force for a beam initially oriented parallel to the magnetic field. Calculations are performed for a beam with a single dipole (solid line); and for beams with multiple dipoles $\kappa = -0.00129$ and spacing of $\rho = 0.2$ (dash line); $\rho = 0.1$ (dot line).

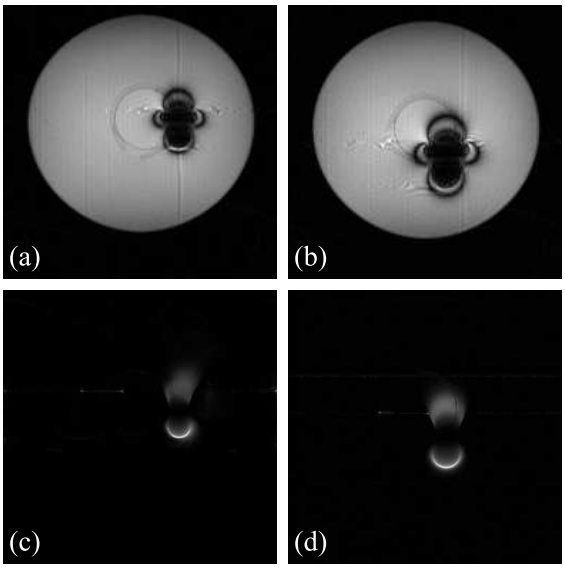


FIG. 9. Artefacts created on coronal images obtained with the TurboFLASH sequence by tips C1 (a) and C2(b); as well with the MS-SET sequence by tips C1 (c) and C2(d). In every image, the field of view is 200 mm by 200 mm.

with a single dipole.

Before concluding, we investigate briefly the effect of using multiple ferromagnetic beads on the imaging and tracking capabilities of the MR scanner. In Fig. 9, images obtained with two types of fast sequences are shown for a catheter with tips C1 (one bead) and C2 (two beads). The TurboFlash images in Fig. 9 of tip C1 (a) and tip C2 are qualitatively similar. The artefact due to the catheter tip with two beads is simply larger than that due to a single bead. With the MS-SET sequence on tip C1 (c) and tip C2 (d), the result is the same. In Fig. 9 (b) and (d) the two ferromagnetic bodies are indistinguishable. They create one large artefact. In a microparticle study [29], it has been shown that for ferromagnetic spheres of similar magnetisation, it is impossible to discern the artefacts of two identical spheres if their spacing is less than 15 times their diameter. Here, the largest spacing tested is 6 times the diameter. For the range of spacing we are interested in, we can thus expect not to see a separation of the artefacts since from afar, the magnetic field of two dipoles close together is the same as that of one stronger equivalent dipole. To give a scale of the images, at the centre of Figs. 9 (a) and (b), we can see the phantom made of a rubber tube shaped into a ring of 80 mm diameter. The scale is the same in (c) and (d) but only the artefact is visible.

V. DISCUSSION AND CONCLUSION

Magnetic gradients combined with the strong permanent magnetic field of a MR scanner can bend in a predictable way a catheter or a guidewire through the use of a newly design tip with a sphere of ferromagnetic material. Moreover, the addition of a second ferromagnetic sphere significantly enhance the amplitude of deformation. However, the extra amplitude of deformation is obtained at the cost of bulkiness as shown on Fig. 2. In the aim of minimising the size of the tip, we investigated the effect of spacing of the magnetic spheres on the dipole-dipole interaction and the torque it generates on the catheter. If the spacing is too small, the interaction creates a strong torque on the catheter tip which leads to the non-linear jump phenomenon. Jumps in amplitude are undesirable since they prevent precise control of the catheter. Moreover, dipole-dipole interactions create a restoring torque that tends to align the catheter with the permanent field. If the magnetic spheres are too close to one another, it hinders navigation away from the direction of the permanent field.

On the other hand, with large enough spacing between the spheres, the deformation curve (5 b-d) remains smooth despite adopting an S-shape. The fact that the displacement is a smooth function of the applied force keeps the control easier for an eventual *in-vivo* application since an increment of force in one direction leads to an incremental displacement in that direction. That is true irrespective of the initial orientation of the catheter.

The addition of a second ferromagnetic sphere at the tip of the catheter does not change qualitatively the shape of the artefact created on MR images. This point is important for the implementation of fast tracking techniques. The two spheres are too close together to be discernible; for all imaging purposes, their magnetic field is equivalent to that of a single dipole. Thus the same MS-SET tracking sequences that have been implemented in the past can be used here. However, by using more ferromagnetic material, the artefact created is larger. This is a significant issue considering that it will be impossible to image the tissues within a few centimetres from

the ferromagnetic body. One possible way around this limitation would be to realise the angiography (either by fluoroscopy or MRI) prior to the insertion of the ferromagnetic body and use it as a road map upon which the tracking data is superimposed [16, 17]. Another possibility would be to equip the guidewire with a ferromagnetic tip small enough so that it can be removed through the lumen of the catheter. This way the ferromagnetic material could be removed from the imaging zone leaving the regular non-magnetic catheter in place. The use of multiple spheres is thus a solution for placing more ferromagnetic material at the tip of the guidewire without increasing its external diameter more than with a single sphere.

In this study, all tests and simulations were performed on catheters or guidewires with clamped-free boundary conditions. These are not representative of in-vivo conditions, where the catheter is in contact with the lumen of the blood vessel at many different points. Future work will focus on catheter steering in phantoms representative of physical anatomy.

[1] P. A. Schneider, *Endovascular Skills: Guidewire and Catheter Skills for Endovascular Surgery* (CRC Press, 2003).

[2] Y. Fu, H. Liu, W. Huang, S. Wang, and Z. Liang, "Steerable catheters in minimally invasive vascular surgery," The International Journal of Medical Robotics and Computer Assisted Surgery **5**, 381–391 (2009).

[3] M. Bock and F. K. Wacker, "MR-guided intravascular interventions: Techniques and applications," Journal of Magnetic Resonance Imaging **27**, 326–338 (2008).

[4] A. Al-Ahmad, J. D. Grossman, and P. J. Wang, "Early experience with a computerized robotically controlled catheter system," Journal of Interventional Cardiac Electrophysiology **12**, 199–202 (2005).

[5] S. Ramcharitar, M. S. Patterson, R. J. van Geuns, C. van Meighem, and P. W. Serruys, "Technology insight: magnetic navigation in coronary interventions," Nature Clinical Practice Cardiovascular Medicine **5**, 148–156 (2008).

[6] T. Krings, J. Finney, P. Niggemann, P. Reinacher, N. Lück, A. Drexler, J. Lovell, A. Meyer, R. Sehra, P. Schauerte, M. Reinges, F. J. Hans, and A. Thron, "Magnetic versus manual guidewire manipulation in neuroradiology: in vitro results," Neuroradiology **48**, 394–401 (2006).

[7] I. Tunay, "Modeling magnetic catheters in external fields," in *Engineering in Medicine and Biology Society, 2004. IEMBS '04. 26th Annual International Conference of the IEEE*, Vol. 1 (2004) pp. 2006–2009.

[8] R. Razavi, D. L. G. Hill, S. F. Keevil, M. E. Miquel, V. Muthurangu, S. Hegde, K. Rhode, M. Barnett, J. van Vaals, D. J. Hawkes, and E. Baker, "Cardiac catheterisation guided by MRI in children and adults with congenital heart disease," The Lancet **362**, 1877–1882 (2003).

[9] D. R. Elgort, C. M. Hillenbrand, S. Zhang, E. Y. Wong, S. Rafie, J. S. Lewin, and J. L. Duerk, "Image-guided and -monitored renal artery stenting using only MRI," Journal of Magnetic Resonance Imaging **23**, 619–627 (2006).

[10] L. W. Bartels and C. J. G. Bakker, "Endovascular interventional magnetic resonance imaging," Physics in Medicine and Biology **48**, R37–R64 (2003).

[11] T.P.L. Roberts, W.V. Hassenzahl, S.W. Hetts, and R.L. Arenson, "Remote control of catheter tip deflection: An opportunity for interventional MRI," Magnetic Resonance in Medicine **48**, 1091–1095 (2002).

[12] F. Settecase, M. S. Sussman, M. W. Wilson, S. Hetts, R. L. Arenson, V. Malba, A. F. Bernhardt, W. Kucharczyk, and T. P. L. Roberts, "Magnetically-assisted remote control (MARC) steering of endovascular catheters for interventional MRI: a model for deflection and design implications," Medical Physics **34**, 3135 (2007).

[13] A. Bernhardt, M. W. Wilson, F. Settecase, L. Evans, V. Malba, A. J. Martin, M. Saeed, T. P.L. Roberts, R. L. Arenson, and S. W. Hetts, "Steerable catheter microcoils for interventional MRIReducing resistive heating," Academic Radiology **18**, 270–276 (2011).

[14] F. Settecase, S. W. Hetts, A. J. Martin, T. P.L. Roberts, A. F. Bernhardt, L. Evans, V. Malba, M. Saeed, R. L. Arenson, and W. Kucharzyk, "RF heating of MRI-Assisted catheter steering coils for interventional MRI," Academic Radiology **18**, 277–285 (2011).

[15] J.-B. Mathieu, S. Martel, L.'H. Yahia, G. Soulez, and G. Beaudoin, "MRI systems as a mean of propulsion for a microdevice in blood vessels," in *Engineering in Medicine and Biology Society, 2003. Proceedings of the 25th Annual International Conference of the IEEE*, Vol. 4 (2003) pp. 3419–3422 Vol.4.

[16] S. Martel, J.-B. Mathieu, O. Felfoul, A. Chanu, E. Aboussouan, S. Tamaz, P. Pouponneau, LH. Yahia, G. Beaudoin, G. Soulez, and M. Mankiewicz, "Automatic navigation of an untethered device in the artery of a living animal using a conventional clinical magnetic resonance imaging system," Applied Physics Letters **90**, 114105 (2007).

[17] A. Chanu, O. Felfoul, G. Beaudoin, and S. Martel, "Adapting the clinical MRI software environment for realtime navigation of an endovascular untethered ferromagnetic bead for future endovascular interventions," Magnetic Resonance in Medicine **59**, 1287–1297 (2008).

[18] J.-B. Mathieu, G. Soulez, G. Beaudoin, O. Felfoul, A. Chanu, and S. Martel, "Abstract no. 76: Steering and tracking of magnetic catheters using MRI systems," Journal of Vascular and Interventional Radiology **19**, S31–S31 (2008).

[19] J.-B. Mathieu, *Étude des paramètres physiques en vue d'applications médicales de l'actionnement magnétique de dispositifs médicaux par un système d'imagerie par résonance magnétique*, Ph.D. thesis, École Polytechnique de Montréal, Montréal, Qc, Canada (2009).

[20] K. Zhang, A. J. Krafft, R. Umathum, F. Maier, W. Semmler, and M. Bock, "Real-time MR navigation and localization of an intravascular catheter with ferromagnetic components," Magnetic Resonance Materials in Physics, Biology and Medicine **23**, 153–163 (2010).

[21] O. Felfoul, J.-B. Mathieu, G. Beaudoin, and S. Martel,

"In vivo MR-Tracking based on magnetic signature selective excitation," Medical Imaging, IEEE Transactions on **27**, 28–35 (2008).

[22] D. C. Jiles, *Introduction to Magnetism and Magnetic Materials, Second Edition*, 2nd ed. (CRC Press, 1998).

[23] J Riegler, B Allain, R J Cook, M F Lythgoe, and Q A Pankhurst, "Magnetically assisted delivery of cells using a magnetic resonance imaging system," Journal of Physics D: Applied Physics **44**, 055001 (2011).

[24] J. P. Reilly, "Peripheral nerve stimulation by induced electric currents: Exposure to time-varying magnetic fields," Medical & Biological Engineering & Computing **27**, 101–110 (1989).

[25] C. L. G. Ham, J. M. L. Engels, G. T. van de Wiel, and A. Machielsen, "Peripheral nerve stimulation during MRI: effects of high gradient amplitudes and switching rates," Journal of Magnetic Resonance Imaging **7**, 933–937 (1997).

[26] K.E. Bisshopp and D.C. Drucker, "Large deflection of cantilever beams," Quarterly of applied mathematics **3**, 272–275 (1945).

[27] R. E. Rosensweig, *Ferrohydrodynamics* (Dover Publications, Mineola, NY, 1997).

[28] S. H. Strogatz, *Nonlinear Dynamics And Chaos: With Applications To Physics, Biology, Chemistry, And Engineering*, 1st ed. (Westview Press, 2001).

[29] N. Olamaei, F. Cheriet, and S. Martel, "Accurate positioning of magnetic microparticles beyond the spatial resolution of clinical mri scanners using susceptibility artifacts," in *EMBC, 2011 Annual International Conference of the IEEE* (2011) forthcoming.